Herausgeber

B. Hamm, Berlin
G. Adam, Hamburg
W. Heindel, Münster
H. Schild, Bonn

C. D. Claussen, Tübingen (Bildessay, Brennpunkt)
M. Forsting, Essen (Neuroradiologie)
T. Helbich, Wien (Der interessante Fall)
J. Lammer, Wien (Interventionelle Radiologie)
G. Staatz, Mainz (Pädiatrische Radiologie)
M. Wucherer, Nürnberg (Technik und Medizinphysik)

Unter Mitwirkung von

H. P. Busch, Trier
F. Diekmann, Berlin
J. Fiehler, Hamburg
R. W. Günther, Aachen
M. Gutberlet, Leipzig
D. Hahn, Würzburg
K. Hausegger, Klagenfurt
M. Heller, Kiel
C. J. Herold, Wien
N. Hosten, Greifswald
W. Hruby, Wien
W. Jaschke, Innsbruck
H.-U. Kauczor, Heidelberg
G. Kauffmann, Heidelberg
K.-J. Klose, Marburg
K.-J. Lackner, Köln
M. Langer, Freiburg
U. Mödder, Düsseldorf
E. Rummeny, München
K. Schwaiger, München
W. Semmler, Heidelberg
W. Steinbrich, Basel
T. J. Vogl, Frankfurt
K.-J. Wolf, Berlin

Redaktionskomitee

T. Albrecht, Berlin
J. Biederer, Kiel
W. Buchberger, Innsbruck
A. Bücker, Homburg/Saar
G. Fürst, Düsseldorf
R. Fischbach, Hamburg
J. Grimm, New York
P. Haage, Wuppertal
C. R. Habermann, Hamburg
A. Heuck, München
M. Horger, Tübingen
T. Jahnke, Kiel
O. Jansen, Kiel
C. Kuhl, Bonn
V. Nicolas, Bochum
C. Nolte-Ernsting, Mülheim/Ruhr
G. Richter, Heidelberg
S. G. Rühm, San Francisco
O. Schäfer, Freiburg
W. Schima, Wien
T. Schmitz-Rode, Aachen
W. Schreiber, Mainz
H. Strunk, Bonn
M. Taupitz, Berlin
M. Uder, Erlangen
M.-M. Uggowitzer, Graz
D. Vorwerk, Ingolstadt
C. Weber, Hamburg
F. Wacker, Berlin
H.-J. Wagner, Berlin
U. Wedegärtner, Hamburg
J. Wildberger, Maastricht

Organ der Deutschen Röntgengesellschaft

Organ der Österreichischen Röntgengesellschaft

In-Vivo Quantification of Wall Motion in Cerebral Aneurysms from 2D Cine Phase Contrast Magnetic Resonance Images

In-Vivo-Quantifizierung der Wandbewegung zerebraler Aneurysmen mittels 2D-Phasen-Kontrast-Magnetresonanztomografie

Autoren   **C. Karmonik[1], O. Diaz[2], R. Grossman[3], R. Klucznik[2]**

Institute   [1] Radiology, The Methodist Hospital Research Institute, Houston
[2] Radiology, The Methodist Hospital, Houston
[3] Neurosurgery, The Methodist Hospital, Houston

Korrespondenzadresse
Dr. Christof Karmonik
Radiology, The Methodist Hospital Research Institute
6565 Fannin MB 1 – 002
77030 Houston
Tel.: ++1/7 13/4 41 15 83
Fax: ++1/7 13/7 90 64 74
ckarmonik@tmhs.org

Zusammenfassung
▼

Ziel: Die quantitative Charakterisierung der Wandbewegung zerebraler Aneurysmen ist von großem Interesse, um ein besseres Verständnis der Ruptierung zu entwickeln, um genauere Computersimulationen durchführen zu können und um theoretische Modelle dieser vaskulären Erkrankungen zu validieren.

Material und Methoden: Mittels Phasen-Kontrast-Magnetresonanztomografie (2D pcMRI) und quantitativer Magnetresonanztomografie (QMRA) wurde die lokale Wandbewegung in sieben zerebralen Aneurysmen in 2 (in einem Falle 3) Querschnittsschichten, welche senkrecht zueinander orientiert wurden, gemessen.

Ergebnisse: Werte für die maximale Wanddehnung reichten von 0,16–1,6 mm (Mittelwert 0,67 mm) und Werte für die maximale Wandkontraktion von −1,91 bis −0,34 mm (Mittelwert −0,94 mm). Im Durchschnitt betrug die Wandauslenkung 0,04–0,31 mm (Mittelwert 0,15 mm). Statistisch signifikante Korrelationen zwischen den Bluteinflusskurven und der Wandauslenkung wurde in 7 der 15 Querschnittsschichten gefunden und in 6 der 15 Querschnittsschichten bestand eine statistisch signifikante Korrelation zwischen der Bewegung des Massenzentrums der Wand und der Einflusskurven (p-value <0,05).

Schlussfolgerung: Mittels Phasen-Kontrast-Magnetresonanztomografie (2D pcMRI) und quantitativer Magnetresonanztomografie (QMRA) kann die Wandbewegung zerebraler Aneurysmen quantifiziert werden; jedoch ist die Anwendung dieser Methode begrenzt durch ihre limitierte räumliche Auflösung.

Abstract
▼

Purpose: The quantification of wall motion in cerebral aneurysms is of interest for the assessment of aneurysmal rupture risk, for providing boundary conditions for computational simulations and as a validation tool for theoretical models.

Materials and Methods: 2D cine phase contrast magnetic resonance imaging (2D pcMRI) in combination with quantitative magnetic resonance angiography (QMRA) was evaluated for measuring wall motion in 7 intracranial aneurysms. In each aneurysm, 2 (in one case 3) cross sections, oriented approximately perpendicular to each other, were measured.

Results: The maximum aneurysmal wall distention ranged from 0.16 mm to 1.6 mm (mean 0.67 mm), the maximum aneurysmal wall contraction was −1.91 mm to −0.34 mm (mean 0.94 mm), and the average wall displacement ranged from 0.04 mm to 0.31 mm (mean 0.15 mm). Statistically significant correlations between average wall displacement and the shape of inflow curves (p-value < 0.05) were found in 7 of 15 cross sections; statistically significant correlations between the displacement of the luminal boundary center point and the shape of inflow curves (p-value < 0.05) were found in 6 of 15 cross sections.

Conclusion: 2D pcMRI in combination with QMRA is capable of visualizing and quantifying wall motion in cerebral aneurysms. However, application of this technique is currently restricted by its limited spatial resolution.

Introduction
▼

The majority of the morphological risk factors for aneurysmal growth and rupture, which have been discussed in the literature (such as aneurysm size, aspect ratio, the ratio of aneurysm ostium area to aneurysm volume [1–4] or aneurysm neck angle [5]), do no take into account temporal changes that occur during the cardiac cycle as these factors are either derived from time-averaged image data (such as 3D digital subtraction angiography [DSA] or 3D time-of-flight [TOF] magnetic resonance imaging [MRI]) or from 2D projection DSA images acquired in a short time period relative to the duration of the cardiac cycle.

Currently, mostly static 3D image data, in particular 3D DSA images, are used to simulate the hemodynamics in cerebral aneurysms for exploring the potential of hemodynamic parameters such as wall shear stresses (WSS) and dynamic pressures as possible predictors for aneurysm growth or rupture [6–16].

At the same time, the pulsatility of cerebral aneurysms of a relatively large amplitude has been reported [17, 18]. Experimental testing has revealed localized variations of stiffness in the aneurysmal wall [19, 20] due to the varying amount of smooth muscle and extra cellular matrix components, primary collagen fibers [21]. A theoretical investigation has recently linked local variations in wall thickness and material stiffness to local stress concentrations and changes in aneurysmal shape [22]. The inhomogeneous distribution of the material properties in the aneurysmal wall may translate into spatially inhomogeneous aneurysmal wall motion when exposed to the varying dynamic pressures occurring during the cardiac cycle.

Theoretical models for aneurysmal wall motion for a better understanding of aneurysm rupture have been proposed: While first models consisted of linear and non-linear versions of Laplace's law [23], more recent approaches employ sophisticated models [24–31].

A fast, readily available, non-invasive in-vivo measurement technique that is capable of quantifying local aneurysm wall motion would be very valuable 1. for providing a means for identifying a wall region of high mobility, 2. for estimating the accuracy of CFD simulations performed with static morphological 3D images, 3. for providing more accurate boundary conditions for CFD simulations other than the now widely used static or rigid walls and 4. as a means to validate and to improve theoretical models that predict aneurysmal wall displacement derived from first principles.

Cine magnetic resonance imaging is routinely used to visualize cardiovascular motion effects [32]. Wall motion in large vessels such as the aorta [33–36] and in small vessels such as the coronaries arteries [37] has been quantified with this method. Motion characteristics of the abdominal aortic aneurysms before and after repair have been reported based on 2D pcMRI measurements [38–40].

In this study, we explored the capability of 2D cine phase contrast magnetic resonance imaging (2D pcMRI) in combination with quantitative magnetic resonance angiography (QMRA) [41] for visualizing and quantifying aneurysmal wall motion in intracranial aneurysms in-vivo. 2D pcMRI does not require contrast injection. It utilizes endogenous contrast between flowing blood and stationary tissue to visualize the aneurysmal lumen and does not expose the patient to ionizing radiation.

Methods
▼

Approval of the institutional review board was obtained for this retrospective study.

Cerebral Aneurysms

Prior to endovascular treatment, 2D pcMRI images were acquired from 7 intracranial aneurysms (in 7 patients). This group of aneurysms included one aneurysm of the anterior communicating artery (AcomA, case 1), one basilar tip aneurysm (BA, case 2) and five aneurysms of the internal carotid artery (ICA, case 3–7) (● Fig. 1). Blebs or lobules were observed in case 1 and cases 5–7. The size of the aneurysm was characterized by the largest aneurysm diameter determined as the maximum of the aneurysm diameters in all cross sections (● Table 1).

2D pcMRI Image Acquisition

2D pcMRI images were prescribed using the QMRA technique as implemented by the NOVA system (Vassol Inc.) [41]. This technique ensures a perpendicular orientation of the 2D pcMRI scan planes relative to the long axis of the artery and therefore to the direction of blood flow (● Fig. 2a). Depending on the length of the cardiac cycle, 12–20 pcMRI images per

Table 1 Parent artery (LACA: left anterior cerebral artery, RACA: right anterior cerebral artery, BA: basilar artery, LICA: left internal carotid artery, RICA: right internal carotid artery), volumetric flow rates (presented as minimum value -maximum value [mean]) and average duration of the cardiac cycle for each case. Largest aneurysm diameter was determined as the maximum diameter of the aneurysm from all cross sections. VENC values are estimated maximum flow velocities.

Tab. 1 Arterie (LACA: left anterior cerebral artery, RACA: right anterior cerebral artery, BA: basilar artery, LICA: left internal carotid artery, RICA: right internal carotid artery), Einflussrate (dargestellt als Bereich Minimum-Maximum [Mittelwert]) und mittlere Länge des Herzzyklus für alle Aneurysmen. Größter Aneurysmendurchmesser ist der größte gemessene Wert von allen Querschnittsflächen. VENC Werte sind geschätzte maximale Flussgeschwindigkeiten.

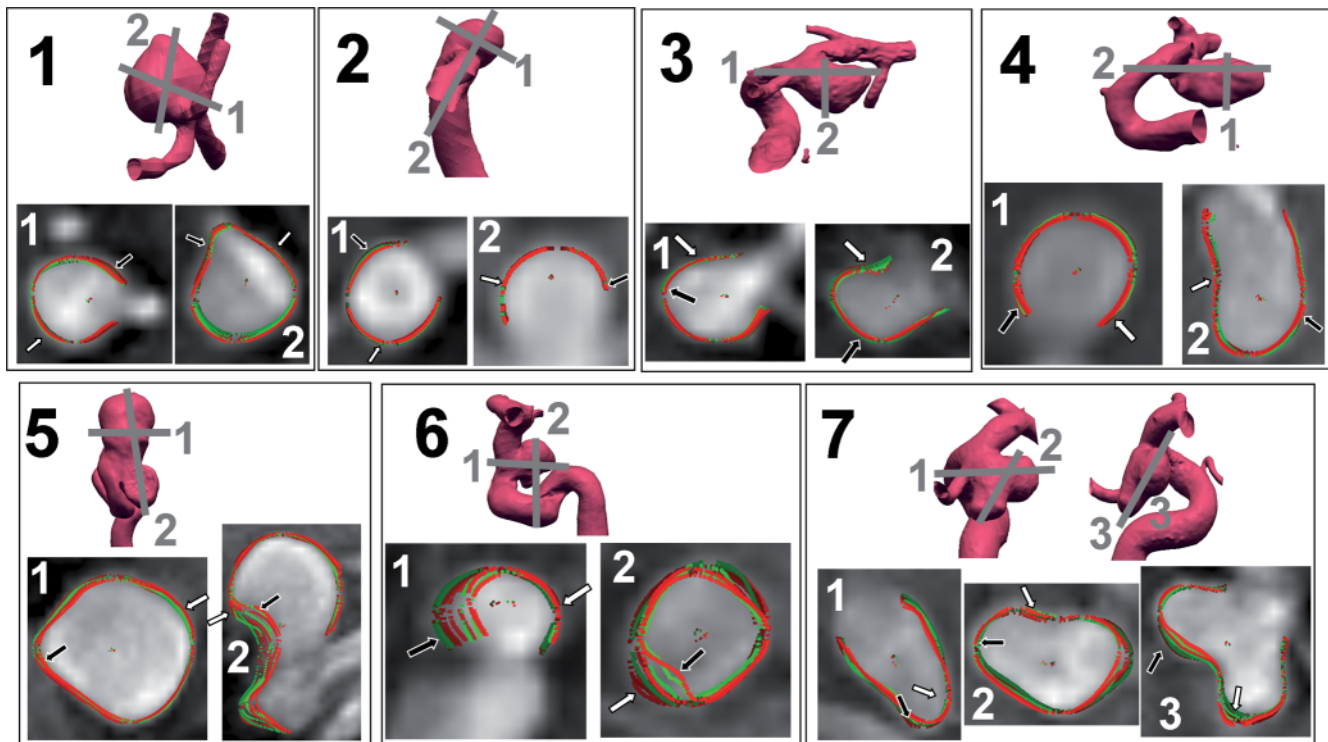| case	parent artery	volumetric blood flow rate [ml/min]	largest aneurysm diameter [mm]	duration of cardiac cycle [ms]	VENC [cm/s]
1	LACA and RACA	83 – 189 (125)	6.7	868	140 and 140
2	BA	140 – 363 (225)	5.8	700	150
3	RICA	196 – 415 (297)	7.6	621	150
4	LICA	190 – 372 (276)	8.8	800	100
5	LICA	214 – 371 (282)	23.7	805	100
6	LICA	153 – 424 (265)	6.4	908	150
7	RICA	188 – 467 (304)	11.1	690	100

Fig. 1 Top of panels: 3D DSA image of aneurysms for cases 1 – 7 with positions of intra-aneurysmal cross sections (gray). Bottom of panels: Overlay of aneurysmal boundaries (as illustrated further in ◐ **Fig. 2**) onto average pcMRI image averaged over all time points. Color coding of the boundaries corresponds to colors in the graph of the volumetric waveform: Accelerating phase from minimum flow to maximum flow green, decelerating flow from maximum to minimum red, see ◐ **Fig. 3**), White arrow marks location of absolute maximum distension and black arrow location of absolute maximum contraction for each cross section.

Abb. 1 Oberes Bildpanel: 3D-DSA-Rekonstruktionen der untersuchten Aneurysmen (1 – 7) mit der Position der aufgenommenen Querschnittsschichten (in grau). Unteres Bildpanel: Überlagerung der segmentierten Wandpositionen (wie in ◐ **Abb. 2** erläutert) auf 2D-pcMRI-Bilddaten konstruiert als Mittelwert aller Bilddaten von einem Herzzyklus. Farbkodierung der Wandpositionen entspricht demselben Farbschema der Einflusskurve: Ansteigender Bereich in grün, absteigender Bereich in rot (◐ **Abb. 3**). Position der maximalen Wandauslenkung ist markiert in weiß, Position der maximalen Wandkontraktion in schwarz.

cardiac cycle were obtained (160 mm field-of-view, matrix: 256 [frequency], 192 [phase], 5 mm slice thickness, interpolated in-plane resolution 0.625 mm). The velocity encoding value (VENC) as the estimated maximum velocity for each measurement was provided by the operator. If the initial VENC value (150 cm/s) proved insufficient by either resulting in images with little contrast between stationary tissue and flowing blood, or if wrap-around (aliasing) flow artifacts were observed, acquisition was repeated with an adjusted VENC value which was chosen by decreasing the initial VENC value in steps of 10 cm/s. Final VENC values ranged from 100 – 150 cm/s for the flow measurements in the parent artery (◐ **Table 1**) and from 60 – 130 cm/s for the intra-aneurysmal cross sections (◐ **Table 2**). Volumetric blood inflow rates into the aneurysms were calculated from the phase difference images of the flow measurements performed at the proximal arterial sections.

Image Post-Processing of Aneurysmal Cross Sections

Images (◐ **Fig. 2b**) were enlarged by a factor of 4 using linear interpolation (◐ **Fig. 2c**) and filtered using a Fourier bandpass filter (NIH ImageJ, [42]) (◐ **Fig. 2 d**) to eliminate spatial frequencies caused by noise (small variations) and image artifacts introduced by inhomogeneous coil sensitivity profiles (large variations). An edge-preserving median filter [43] was then applied to reduce image grayscale inhomogeneities inside the lumen (◐ **Fig. 2e**). The median-filtered images showed a

strong contrast between the aneurysmal lumen and the surrounding stationary tissue and the aneurysmal lumen boundaries could therefore be segmented by single value thresholding (◐ **Fig. 2f**). The aneurysmal lumen boundary was separated from the lumen of the parent artery (if present in the image) by a straight line drawn by the operator. This manually drawn boundary section was excluded from the following wall motion analysis.

The luminal wall boundaries were color-coded with the same color scheme as the inflow waveform (◐ **Fig. 2 h, i**). An overlay image was created containing all the wall boundaries together with an average pcMRI image for illustrating temporal aneurysm wall boundary motion (◐ **Fig. 2j**).

Aneurysmal Wall Motion Analysis
Aneurysm Center Point Motion

Please also see figure 3 for a graphical visualization of the geometrical parameters defined in the following section.

The motion of the aneurysm as a whole will be most likely influenced by pulsatile movements of the cerebral vascular tree. To separate this motion from wall motion components relative to the center of the aneurysm, the center of the aneurysmal lumen boundary (ALC) was calculated separately for each time point in the cardiac cycle where an image was acquired and a 2D polar coordinate system was defined for each time point with the ALC as the origin. The pulsatile movement of the aneurysm as a whole and in relation to the vascular tree
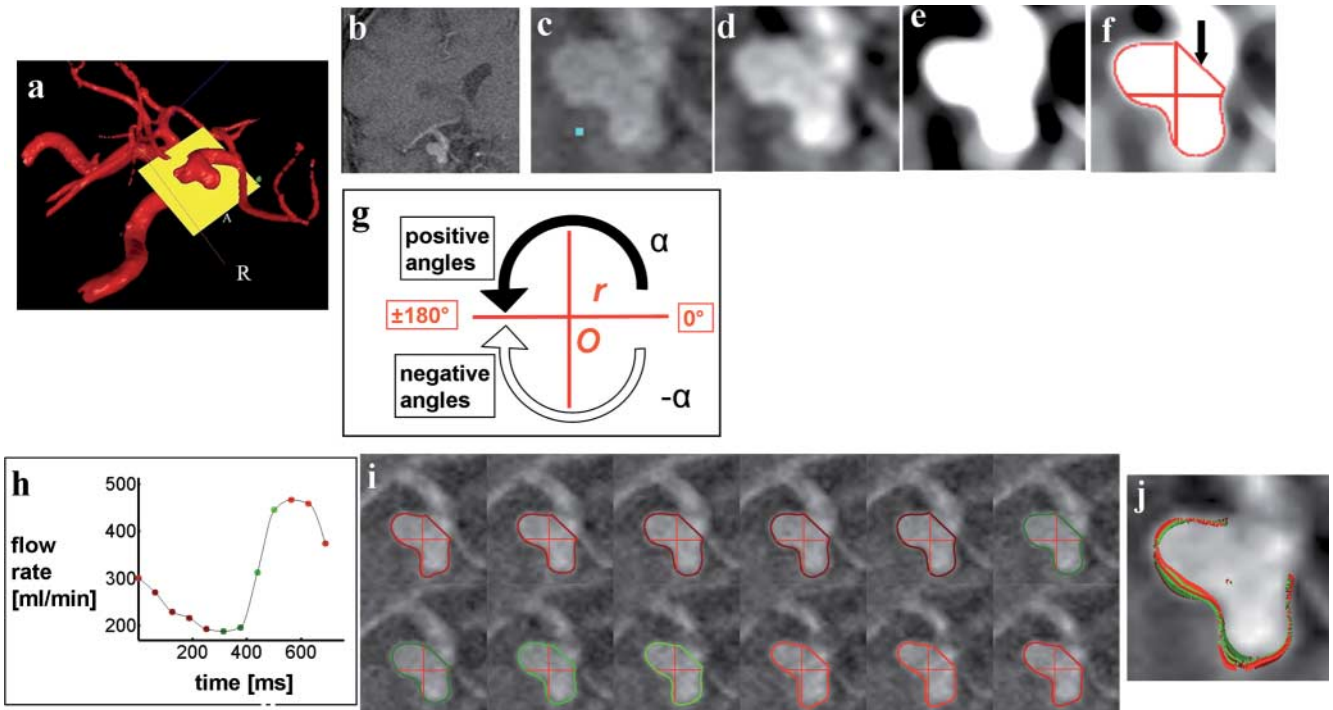
Fig. 2   a Screen capture of a 3D surface reconstruction of cerebral vasculature with prescribed intra-aneurysmal cross section (NOVA, Vassol Inc.) b–f Image sequence illustrating the pre-processing of the original pcMRI magnitude images(b). Enlarged images (factor 4, linear interpolation [c]), FFT-filtered (d), filtered with median filter (e). Median filtered image with segmented aneurysm boundary (red curved line) and axes of coordinate system (red straight lines) (f). Aneurysm boundary to the parent artery was marked by the user (black arrow) and not included in the aneurysm wall motion analysis. Blue square marks original pixel size of the acquired pcMRI image data in the enlarged magnitude image. g Schematic of coordinate system defining distance r of aneurysmal boundary points from origin O (center of the coordinates of all aneurysmal boundary points) and angle α denoting angular position of each boundary point. h Inflow waveform for case 6 color-coded (green: accelerating phase from minimum inflow to maximum inflow, red: decelerating phase from maximum inflow to minimum inflow). i Corresponding thresholded 2D pcMRI magnitude images to (h) with aneurysm boundary (boundary colors correspond to colors in [h]). j Overlay of color-coded aneurysmal boundaries onto average pcMRI image averaged over all time points for visualizing aneurysms wall boundary motion during the cardiac cycle.

Abb. 2   a Dreidimensionale Rekonstruktion der zerebralen Vaskulatur zur Illustration der Positionen der aufgenommen 2D-pcMRI-Schichten (gelb). b–f Bilderfolge welche die Schritte der Bildverarbeitung der originalen 2D-pcMRI-Bilddaten veranschaulicht. b Um Faktor 4 linear interpolierte Bilddaten, c FFT gefiltert, d nach Anwendung des Median Filters, e gefilterte Bilddaten überlagert mit der Position der segmentierten Wandposition des Aneurysma, schwarze Markierung zeigt die Abgrenzung der Aneurysma zur Arterie (nicht berücksichtigt in der Analyse der Wandbewegung). Blaue Rechtecke veranschaulichen die räumliche Auflösung in den Originalbilddaten. g Veranschaulichung des gewählten Koordinatensystems welches die Distanz r der Wandpunkte von dem Zentrum O zeigt zusammen mit dem Polarwinkel α. h Einflusskurve für Aneurysma 6 mit Farbkodierung (grün: ansteifender Fluss, rot: absteigender Fluss). i Wandpositionen kodiert entsprechend dem Farbschema in h überlagert auf 2D-pcMRI-Bilddaten für alle Bilddaten des Herzzyklus. j Wandpositionen kodiert entsprechend dem Farbschema in h überlagert auf 2D-pcMRI-Bilddaten gemittelt über den gesamten Herzzyklus.

was then decoupled from the relative wall motion measured relative to the origin of the polar coordinate system. The average maximum displacement of the ALC was calculated for all cross sections and for all time points as an approximation of the global motion of the whole aneurysm. The correlation of the time-dependent ALC displacement with the inflow waveform was calculated using the Pearson correlation coefficient r_{ALC} (statistical significance was established with $p < 0.05$).

Maximum Distention and Contraction

Each aneurysmal boundary point was characterized by a radial coordinate (distance r) and an angular coordinate (azimuth angle α) (Fig. 2 g) in the 2D polar coordinate system with the ALC as the previously defined origin (see previous section). The displacement for each boundary point perpendicular to the lumen boundary was then calculated as the difference of r at a certain time point and of r0 at the time of minimal inflow. The maximum distention (d_{max}, positive) and maximum

contraction (d_{min}, negative) for all times were determined for each boundary point as well as the maxima of these parameters for all points (Fig. 3).

Average Wall Displacement

The average displacement (d_{ave}) was defined as the temporal average over all displacements of all boundary points. The temporal standard deviation of d_{ave} (Δd_{ave}) was assumed to be a measure of the variation for the aneurysmal wall motion occurring during the cardiac cycle.

Localized Wall Motion

Due to local variations in biomechanical parameters of the aneurysmal wall, a localized heterogeneous wall motion might be expected. To provide a measure for this heterogeneity, we introduced the following two quantities: the ratio of the number of positive (r_{pos}) and negative (r_{neg}) significant correlations (p-value ≤ 0.05) relative to the total number of boundary
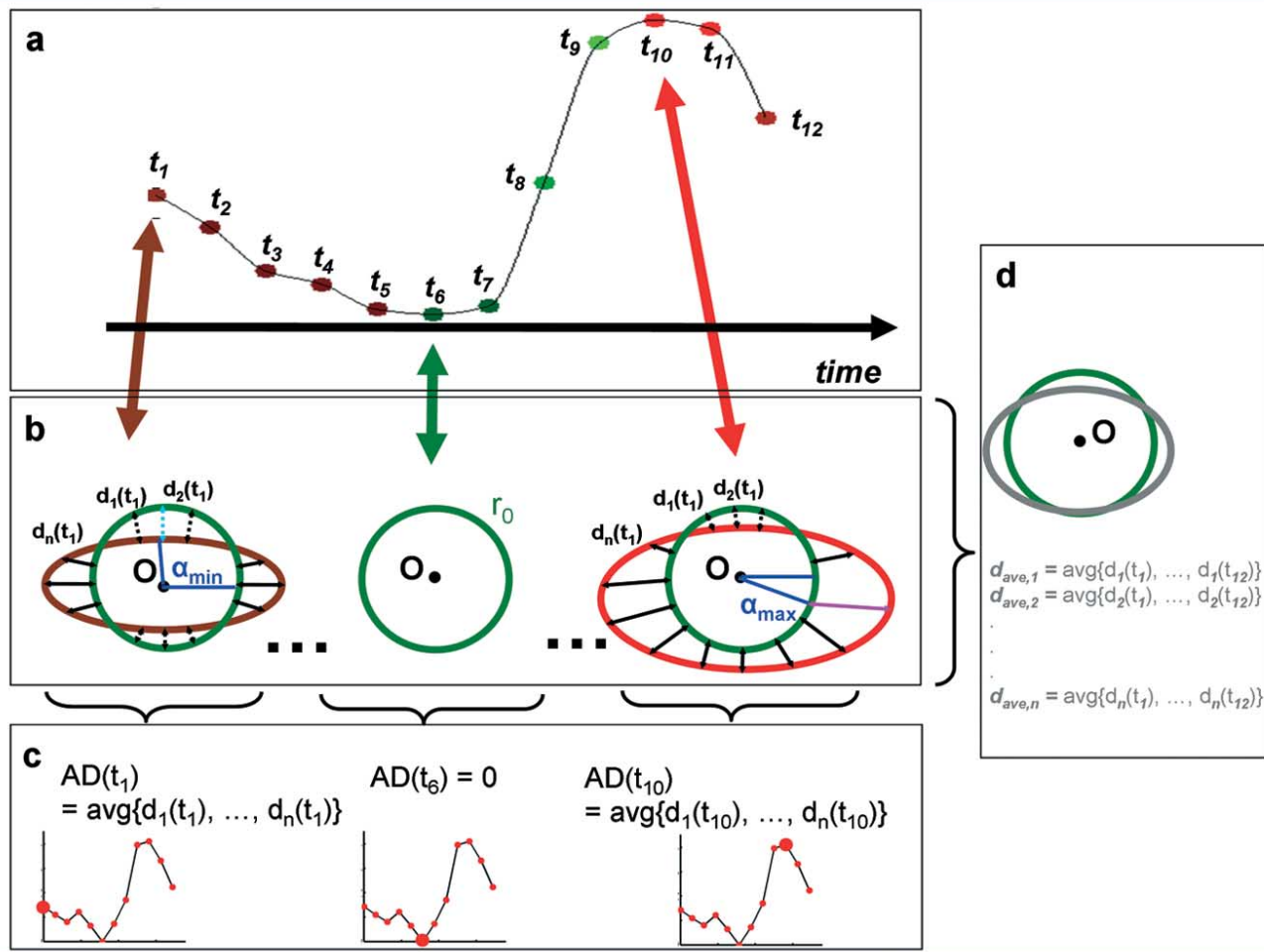
Fig. 3 Schematic illustration of wall motion analysis: **a** Volumetric inflow waveform measured at 12 time points t1–t12. green colors: acceleration phase from minimum to maximum inflow, red colors: deceleration phase from maximum inflow to minimum inflow. **b** Corresponding schematic aneurysm boundaries for representative time points color-coded according to color scheme for the volumetric inflow waveform: Center (green): wall boundary at minimum inflow (r_0), left (dark red): wall boundary at average inflow superimposed on wall boundary for minimum inflow, right (bright red): wall boundary at maximum inflow superimposed on wall boundary for minimum inflow. Origin of wall boundaries is denoted by O, wall distention and wall contractions $d_i(t)$ (i: boundary point index, i = 1,...,n) are indicated by filled and dashed lines respectively. Maximum contraction d_{min} is shown in bright blue (in left image), and maximum distention d_{max} is shown in pink (in right image). Angles for maximum distention and maximum contractions, α_{max} and α_{min}, respectively, are shown in dark blue. **c** Illustration of calculation of the total averaged displacement for one time point AD(t) for the three time points in **b** as average value over all $d_i(t)$, i = 1,...,n. Each time point is marked in bold in the graph for AD(t) in the lower part of the panel. **d** Schematic time-averaged wall boundary (gray) superimposed on the wall boundary for minimum inflow (green), origin is denoted by O. The time averaged displacement $d_{ave,i}$ for each boundary point i is calculated as the average over all time points, maximum d_{max} and d_{min} were found as maxi-

mum and minimum (negative), respectively, of all $d_i(t_k)$, i = 1,...,n; k = 1, ...,12 and d_{ave} was the average of all $d_{ave,i}$.

Abb. 3 Schematik, welche die Berechnung der Wandbewegung illustriert: **a** Einflusskurve gemessen an 12 Zeitpunkten $t_1 - t_{12}$ In grün: ansteigender Blutfluss, in rot: abfallender Blutfluss. **b** Idealisierte Wandposition der Aneurysmawand in den Querschnittsschichten für drei representative Zeitpunkte (Farbgebung korrspondiert mit Farbschema der Einflusskurve). Mitte (grün): Wandposition (r_0) für minimalen Einfluss, links (braun): Wandposition zu einem Zeitpunkt mittleren Einflusses, rechts (rot): Wandposition zu dem Zeitpunkt maximalen Einflusses. Das Massenzentrum der Wandpunkte ist mit O markiert, Wandausdehnung (- – -) and Wandkontraktion (——) für individuelle Punkte sind $d_i(t)$ (i: Indizes der Wandpunkte i, i = 1,...,n). Maximale Wanddehnung d_{max} für alle Wandpunkte ist veranschaulicht in hellrot, maximale Wandkontraktion d_{min} für alle Wandpunkte in hellblau. Korrespondierende Winkelpositionen α_{max} und α_{min} sind in dunkelblau eingezeichnet. **c** Veranschaulichung der Berechnung von AD(t) als Mittelwert aller Wandbewegungen $d_i(t)$ und markiert in der grafischen Darstellung von AD(t) als größeres Symbol. **d** Positionen der mittlere Wanddehnung (grau) $d_{ave,i}$ wurden bestimmt als zeitlicher Mittelwert und die mittlere Wandbewegung ist der Mittelwert aller $d_i(t_k)$.

points. They represent the fraction of the aneurysmal lumen boundary which moves in phase (r_{pos}) and the fraction which moves out-of-phase (r_{neg}) relative to the inflow waveform. If the wall motion consists of a global distension during maximum inflow followed by a global contraction during minimum inflow, r_{pos} would be expected to be close to unity and r_{neg} would be close to zero (no wall fraction moves out-of-phase). The difference angle of the angles of maximum distention (α_{max}) and maximum contraction (α_{min}) $\Delta\alpha = \alpha_{max} - \alpha_{min}$ was determined to characterize the locations of the maximal distention and maximal contraction relative to each other.
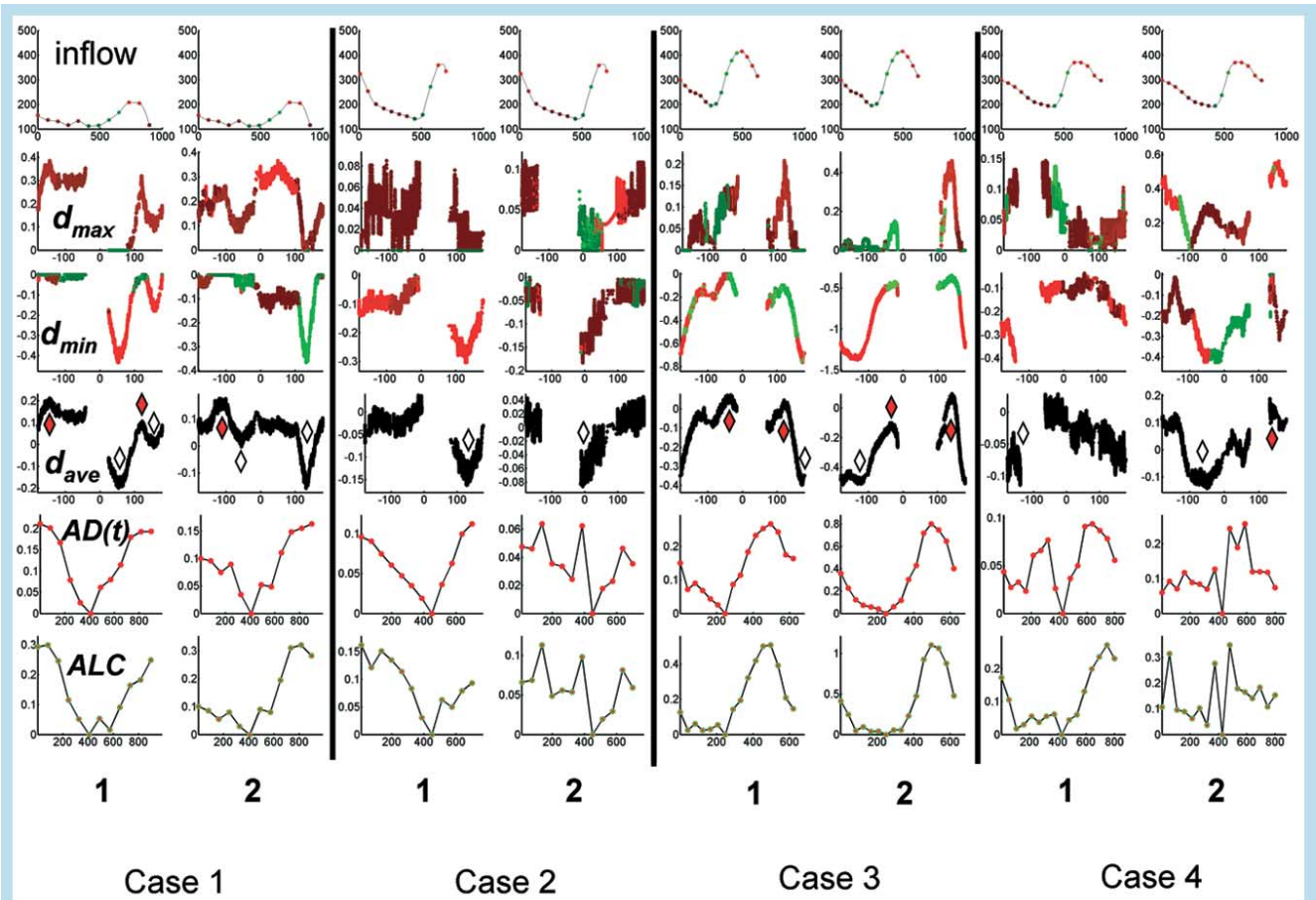
Fig. 4 Inflow volumetric waveform (inflow), maximum distention (d_{max}), maximum contraction (d_{min}), average displacement (d_{ave}), temporal average displacement (AD(t)) and displacement of the center of the aneurysm lumen boundary (ALC) for the cross sections (1 or 2) of case 1 – 4. Red and white symbols denote locations of local maxima and local minima of d_{ave}, respectively. Color coding in the plots of d_{max}, and d_{min} corresponds to the color coding in the plot of the volumetric inflow waveform (inflow) and allows so to identify the time of maximum distention and maximum contraction for section of the aneurysmal wall.

Abb. 4 Einflusskurven (inflow), maximale Wanddehnung (d_{max}), maximale Wandkontraktion (d_{min}), mittlere Wandbewegung (d_{ave}), zeitgemittelte mittlere Wandbewegung (AD(t)) und Bewegung des Massenzentrums der Wandpunkte (ALC) für die Querschnittsflächen (1 oder 2) der Aneurysmen 1 – 4. Rote und weiße Symbole bezeichnen lokale Maxima und Minima der mittleren Wandbewegung. Farbgebung für d_{max} und d_{min} korrespondiert mit dem Farbschema der Einflusskurven.

Total Average Displacement

The total average displacement for all boundary points AD(t) was calculated as an average over all displacements of all boundary points for time t. This parameter was introduced to quantify the relative wall motion averaged over all boundary points during the cardiac cycle. If the wall motion is homogeneous and driven by blood inflow, maximum distension for all boundary points should be observed close to the time of maximum inflow and consequently maximum contraction during the time of minimum inflow. In this case, the shape of AD(t) should closely follow the shape of the inflow waveform. To quantify the similarity in the shape of both curves, the correlation coefficient $r_{AD(t)}$ of AD(t) with the inflow waveform was determined with the Pearson correlation coefficient (statistical significance with a p-value < 0.05).

Results
▼
Volumetric Inflow Rates

The average flow rates for case 1 (125 ml/min; combined inflow from both anterior cerebral arteries (AcomA)) and case 2 (225 ml/min; BA) were each lower than the average flow rates in each of the remaining cases (the mean flow rate for cases 3 – 7 was 285 ± 16 ml/min; ICA) (● **Table 1**).

Aneurysm Wall Motion
Aneurysm Center Point Motion

The average maximum ALC displacement was lowest for case 2 (0.14 mm) and highest for case 3 (0.81 mm) (● **Table 2**). In general, the ALC followed the shape of the inflow waveform (exception: cross sections 2 for case 2 and case 4 and cross sections 1 for case 1 and case 5, figures 4 and 5). A statistically significant positive correlation between both curves was found for 6 cross sections (● **Table 2**).

Maximum Distention and Maximum Contraction

Maximum d_{max} ranged from 0.09 mm (case 2) to 1.60 mm (case 5) and also varied largely within the cross sections from the same aneurysm, with the largest variation being 1.03 mm for case 5. Similar behavior for the maximum of d_{min} was observed, with a largest (negative) value of –1.70 mm (case 5) and a smallest (negative) value of –0.18 mm (case 2). Case 5 showed the largest variation within the cross sections (1.14 mm). For all cross sections, a moderate trend of a linear correlation between the maximum values of d_{max} and d_{min} was found ($R^2 = 0.55$, ◗ **Fig. 6**) (◗ **Table 3**).

Average Wall Displacement

d_{ave} ranged from 0.3 mm (case 3, cross section 2) to 0.04 mm (case 4, cross section 1). The relatively large standard deviation d_{ave} for the average displacement d_{ave} indicates a heterogeneous wall motion with high amplitudes.

Localized Wall Motion

The ratios r_{pos} and r_{neg} varied for different aneurysms and also within the cross sections for the same aneurysm. The largest portion of the aneurysmal wall moving in phase with the inflow waveform was 52 % (cross section 1 of case 1) and the largest portion of the aneurysmal wall moving out-of-phase was 79 % (cross section 1 of case 4). The local heterogeneity of the wall motion can be appreciated particularly in cross section 3 for case 7 in ◗ **Fig. 1**. The distal wall of both lobes moves out-of-phase with respect to each other as visualized by the alternating red and green wall boundaries. These results indicate that a more heterogeneous localized wall motion might dominate instead of a global wall motion only, demonstrating a more elastic behavior in terms of wall biomechanics in all cases modulating the global aneurysmal bulk motion.

The values for α_{max} and α_{min} were similar in three cross sections ($\Delta\alpha = 5°$ in cross section 2 for case 5, $\Delta\alpha = 4°$ cross section 2 for case 6 and $\Delta\alpha = 28°$ cross section 1 for case 7), thus identifying a portion of the aneurysmal wall with high local pulsatility of opposing large amplitudes. In all three cases, the so identified wall section coincided with the location of a lobule or bleb (◗ **Fig. 1**). The values for α_{max} and α_{min} were different for the remaining cases (in particular $\Delta\alpha = 174°$ in cross section 2 of case 4), thus indicating a more global pulsation involving the entire aneurysm.

Total Average Displacement

The shape of the AD(t) curves (◗ **Fig. 4** and **5**) resembled the shape of the inflow waveform with varying degrees (exception: cross section 2 for case 2 and cross section 1 for case 5). Significant correlations between the two curves were found at least for one cross section for each of the aneurysms of the ICA (with correlation coefficients ranging from 0.52, case 4 to 0.68, case 3) (◗ **Table 4**).

Table 2 Average maximum ALC displacement and correlation coefficient of the temporal variation of ALC with the inflow waveform. Statistical significant correlation is marked in bold. VENC values are estimated flow velocities.
Tab. 2 Mittelwert der maximalen ALC und Korrelationskoeffizient der zeitlichen Variation von ALC mit der Einflusskurve. Statistische Signifikanz ist in Fettdruck. VENC-Werte sind geschätzte Flussgeschwindigkeiten.

case	average maximum ALC displacement [mm]	correlation coefficient r_{ALC}	VENC [cm/s]
1	0.31	1: –0.3	80
		2: 0.8	80
2	0.14	**1: –0.7**	60
		2: –0.3	60
3	0.81	**1: 0.7**	100
		2: 0.7	100
4	0.31	**1: 0.6**	80
		2: 0.1	80
5	0.44	1: 0	150
		2: 0.5	80
6	0.75	1: 0.5	130
		2: 0	130
7	0.61	1: 0.5	60
		2: 0.4	60
		3: 0.6	100

Table 4 Maximum d_{max}, maximum d_{min} and average displacement ($d_{ave} \pm$ standard deviation d_{ave}), fraction of aneurysmal boundary moving in (r_{pos}) and opposite (rneg) phase relative to the volumetric inflow waveform and difference angle of α_{max} and α_{min} ($\Delta\alpha$).
Tab. 4 Maximale d_{max}, maximale d_{min} und $d_{ave} \pm d_{ave}$, Fraktionen der Aneurysmenwand mit positiver (r_{pos}) oder negativer (r_{neg}) Phase relativ zu der Einflusskurve und Differenz von α_{max} und α_{min} ($\Delta\alpha$).

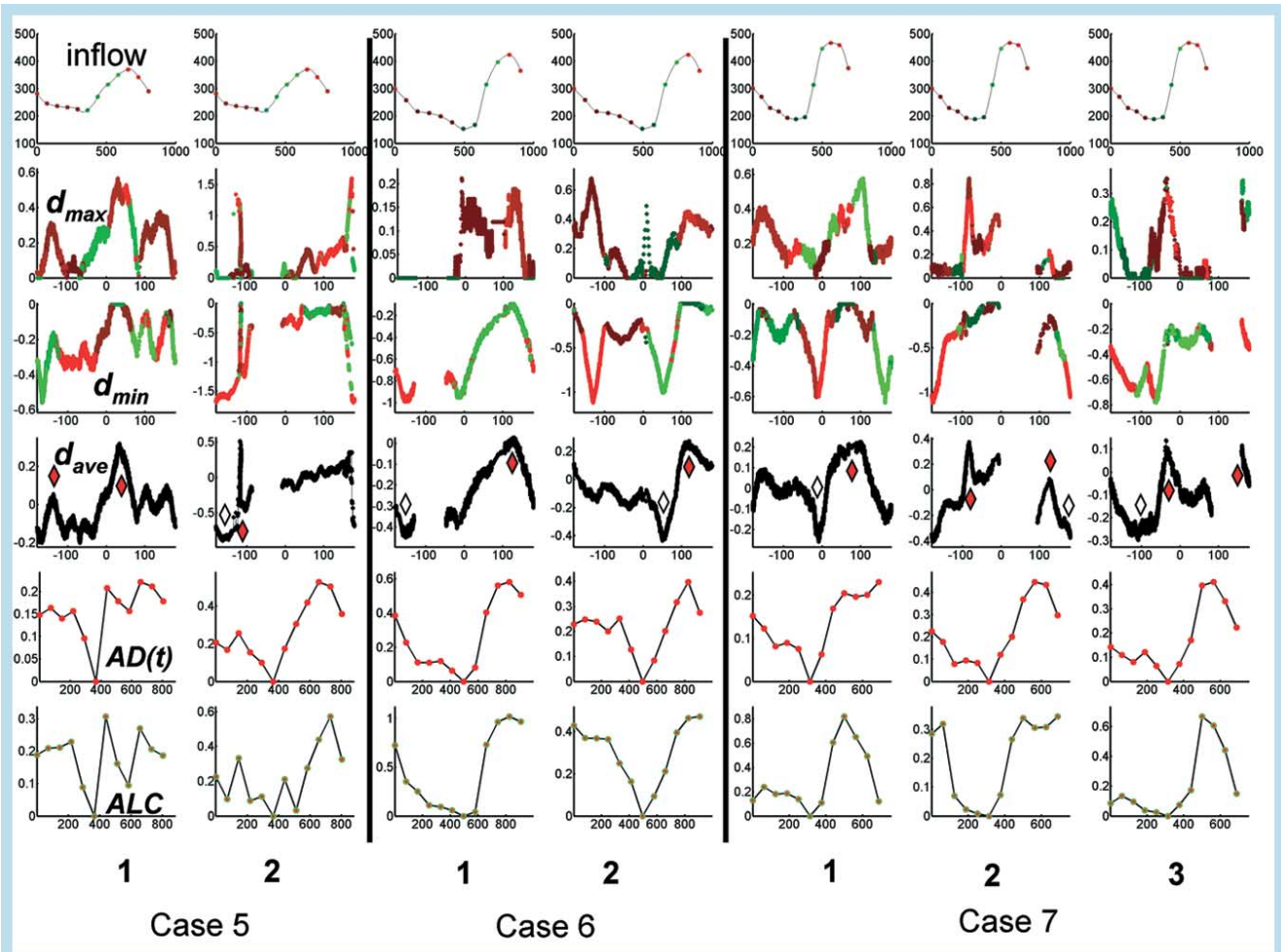| case	cross section	d_{max} [mm]	d_{min} [mm]	d_{ave} [mm] ± d_{ave}[mm]	r_{pos}	r_{neg}	$\Delta\alpha$[°]
1	1	0.39	–0.43	0.12 ± 0.06	0.52	0.23	161
	2	0.37	–0.37	0.07 ± 0.03	0.34	0.29	82
2	1	0.09	–0.30	0.05 ± 0.05	0	0.22	124
	2	0.11	––0.18	0.03 ± 0.02	0.55	0.36	164
3	1	0.21	–0.76	0.12 ± 0.11	0.06	0.21	53
	2	0.46	–1.38	0.30 ± 0.16	0.07	0.04	87
4	1	0.15	–0.42	0.04 ± 0.03	0.03	0.79	84
	2	0.56	–0.43	0.08 ± 0.04	0.25	0.29	174
5	1	0.57	–0.56	0.10 ± 0.08	0.23	0.28	163
	2	1.60	–1.70	0.20 ± 0.22	0.17	0.29	5
6	1	0.21	–0.99	0.24 ± 0.13	0	0.17	143
	2	0.68	–1.12	0.17 ± 0.09	0.21	0.47	4
7	1	0.35	–0.78	0.15 ± 0.08	0.04	0.14	28
	2	0.58	–0.64	0.08 ± 0.06	0.42	0.22	57
	3	0.85	–1.12	0.19 ± 0.11	0.18	0.12	95

Fig. 5 Inflow volumetric waveform (inflow), maximum distention (d_{max}), maximum contraction (d_{min}), average displacement (d_{ave}), temporal average displacement AD(t) and displacement of the center of the aneurysm lumen boundary (ALC) for the cross sections (1, 2 or 3)for case 5 – 7. Red and white symbols denote locations of local maxima and local minima of d_{ave}, respectively Color coding in the plots of d_{max},and d_{min} corresponds to the color coding in the plot of the volumetric inflow waveform (inflow) and allows so to identify the time of maximum distention and maximum contraction for section of the aneurysmal wall.

Abb. 5 Einflusskurven (inflow), maximale Wanddehnung (d_{max}), maximale Wandkontraktion (d_{min}), mittlere Wandbewegung (d_{ave}), zeitgemittelte mittlere Wandbewegung (AD(t)) und Bewegung des Massenzentrums der Wandpunkte (ALC) für die Querschnittsflächen (1, 2 oder 3) der Aneurysmen 5 – 7. Rote und weiße Symbole bezeichnen lokale Maxima und Minima der mittleren Wandbewegung. Farbgebung für d_{max} und d_{min} korrespondiert mit dem Farbschema der Einflusskurven.

Discussion
▼

In 7 intracranial aneurysms (one AcomA aneurysm, one basilar tip aneurysm and 5 aneurysms of the ICA), intra-aneurysmal cross sections were recorded at different time points in the cardiac cycle using 2D pcMRI and QMRA.

The technique of 2D pcMRI has recently been shown to be capable of providing flow information in arteries of the cerebral circulation in combination with QMRA with an accuracy of 4.5% when compared to flow phantom measurements [44]. The volumetric inflow rates measured in this study (○ **Table 1**, RACA: 54 ml/min, LACA: 93 ml/min, RICA: 301 ml/min (average for cases 3 and 7), LICA: 274 ml/min (average for cases 4 and 6) are in good agreement with values reported in the literature obtained from 83 volunteers (LICA = 264 ± 52 ml/min, RICA 252 ± 52 ml/min, RACA 80 ± 28 and LACA 85 ± 26 ml/min) except for BA in case 2 (225 ml/min, literature value: BA 131 ± 40 ml/min) [44]. Cerebral aneurysms have been previously investigated using magnetic resonance angiography [45, 46] and 2D pcMRI. In a

study performed by Zhu et al. of 26 large (15 to 39 mm) cerebral aneurysms, pcMRI was found to successfully differentiate blood flow from static tissue and in combination with contrast-enhanced MRI was capable of demonstrating the geometry of these aneurysms [47]. Myer at al. conducted an early study of 15 cerebral aneurysms with pcMRI and detected a 51% ± 10% increase in volume between systole and diastole in 6 ruptured aneurysms compared with a 17.6% ± 8.9% increase in volume in 10 unruptured aneurysms (p < 0.005) [17].

Ishida et al. visualized motion of the aneurysmal wall, bleb and dissecting cavity in movies created from 4D computed tomographic angiographic acquisitions [18]. Pulsating blebs were detected in nine of 28 investigated saccular aneurysms. In two patients with subarachnoid hemorrhage, preoprative 4D CT angiography revealed pulsating blebs that were confirmed as rupture points during the surgical procedure. While no quantitative analysis of this pulsation was performed, the maximum amplitude of the pulsating wall sections can be estimated from the 4D CT movies to be in the order of millimeters. Aneurysms of

Table 4 Correlation coefficient of AD(t) with the waveform of the volumetric inflow rate. Statistical significant correlation is marked in bold.
Tab. 4 Korrelationskoeffizient von AD(t) mit der Einflusskurve. Statistische Signifikanz ist in Fettdruck.

case	correlation coefficient $r_{AD(t)}$
1	1: 0.04
	2: 0.48
2	1: −0.04
	2: −0.39
3	**1: 0.66**
	2: 0.68
4	**1: 0.52**
	2: 0.34
5	1: 0.38
	2: 0.67
6	1: 0.53
	2: 0.21
7	**1: 0.59**
	2: 0.64
	3: 0.65

Fig. 6 Plot of maximum d_{max} versus maximum d_{min} for all cross sections. A linear relationship as indicated by the straight line ($R^2 = 0.55$) can be appreciated.

Abb. 6 Plot des maximalen d_{max} und maximalen d_{min} für alle Querschnitts-schichten. Ein linearer Zusammenhang ist veranschaulicht durch die gezeigte Gerade ($R^2 = 0,55$).

cases 5 – 7 in our study also exhibited blebs. A large amplitude for the wall motion (up to 1.7 mm) was found at the location of these blebs in agreement with the observation of Ishida et al. Intuitively, the motion of the aneurysmal wall may be expected to correlate with the dynamic pressure and therefore with the volumetric inflow waveform. Such a motion would result in global distention of the aneurysmal wall for maximum inflow compared to minimum inflow. While such a trend can be observed in the time dependency of AD(t) for the majority of the investigated cross sections (exceptions are cross section 2 of case 2 and cross section 1 of case 4), the more detailed analysis of the wall motion as given by d_{max}, d_{min} and d_{ave} reveals complicated heterogeneous local motions of segments of the aneurysmal boundaries in all cross sections (○ **Fig. 4** and **5**) in accordance with the reports of a heterogeneous composition of the aneurysmal wall [19 – 21] implying a significant degree of mechanical anisotropy [48]. The moderate linear correlation found between maximum contraction and maximum distention may be indicative of a global material property of the aneurysm wall modulated by local wall anisotropies (○ **Fig. 6**).

The observed wall motion may also be influenced by other factors than intrinsic properties, most importantly by the structure of the peri-aneurysmal environment. San Millan Ruiz et al. have demonstrated that the existence of contact constraints between intracranial saccular aneurysms and the peri-aneurysmal environment influences the shape and risk of aneurysm rupture [49].

The amplitude of the motion of the aneurysmal boundary points relative to each other were found to be relatively large compared to the aneurysm size (○ **Table 1**) and may have a strong influence on the calculated hemodynamic parameters, in particular the WSS. Results of CFD simulations, if assuming rigid walls as the boundary condition, may have to be interpreted with caution and the incorporation of fluid structure interactions might be necessary for modeling aneurysms with high wall pulsatility.

The limitations of this study are the relatively low spatial resolution of 2D pcMRI compared to aneurysm size. MR scanners with a higher field strength (3 T or higher) and a consequently higher sign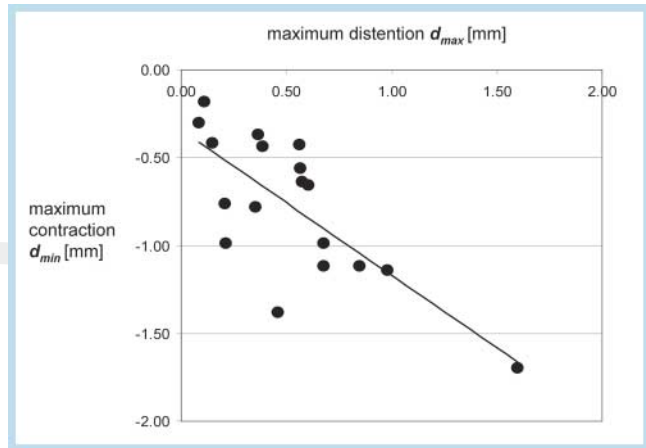al-to-noise ratio (SNR) will enable the use of a higher in-plane resolution and/or a thinner slice thickness for imaging smaller aneurysms or smaller features of larger aneurysms (such as daughter aneurysms and small blebs) or the effect of particular geometries of the parent artery such as fenestrations [50]. Low blood flow velocities inside the aneurysm combined with an alteration of the intra-aneurysmal flow pattern during diastole compared to systole could lead to flow voids in the 2D pcMRI images which could be interpreted as changes in aneurysm shape. Results from CFD simulations and measurements of intra-aneurysmal flow patterns, however, have demonstrated that blood flow patterns inside the aneurysms remain laminar and do not change significantly during the cardiac cycle and that the blood velocities scale with those in the parent artery [16]. Flow voids due to these effects leading to misinterpretations of the aneurysm wall motion can therefore be excluded in the 2D pcMRI images.

To achieve higher spatial (and temporal) resolution, either the acquisition time has to be increased (to compensate for the lack of signal to noise) or special equipment (surface coils) or pulse sequences currently not approved for clinical application may have to be used. For this purpose, a prospective study should be designed incorporating the use of dedicated research equipment and pulse sequences.

Continued advances of 2D pcMRI imaging especially with 4D imaging methods are encouraging. First qualitative results of the visualization of 3D aneurysmal wall motion in cerebral aneurysms using 4D pcMRI imaging have been reported in an animal model [51] and in-vivo [52, 53]. These technical advances emphasize the growing potential of magnetic resonance imaging for characterizing aneurysm morphology, motion and hemodynamics.

Conclusion
▼

Aneurysmal wall motion in 2D intra-aneurysmal cross sections obtained with 2D pcMRI and QMRA were visualized and quantified. Locally heterogeneous wall motion was observed, and large amplitudes of displacement at the position of blebs or lobules

were noted. These results may be of importance for assessing the risk of aneurysm rupture, for providing more accurate boundary conditions for CFD simulations and as reference data for theoretical models describing aneurysmal wall motion.

Acknowledgement
▼

References

1 *Black SP, Leo HL, Carson WL.* Recording and measuring the interior features of intracranial aneurysms removed at autopsy: method and initial findings. Neurosurgery 1988; 22: 40–44

2 *Ma B, Harbaugh RE, Raghavan ML.* Three-dimensional geometrical characterization of cerebral aneurysms. Ann Biomed Eng 2004; 32: 264–273

3 *Ujiie H, Tachibana H, Hiramatsu O et al.* Effects of size and shape (aspect ratio) on the hemodynamics of saccular aneurysms: a possible index for surgical treatment of intracranial aneurysms. Neurosurgery 1999; 45: 119–129, discussion 129–130

4 *Ujiie H, Tamano Y, Sasaki K et al.* Is the aspect ratio a reliable index for predicting the rupture of a saccular aneurysm? Neurosurgery 2001; 48: 495–502, discussion 502–493

5 *Karmonik C, Arat A, Benndorf G et al.* A technique for improved quantitative characterization of intracranial aneurysms. AJNR 2004; 25: 1158–1161

6 *Mantha A, Karmonik C, Benndorf G et al.* Hemodynamics in a cerebral artery before and after the formation of an aneurysm. AJNR 2006; 27: 1113–1118

7 *Acevedo-Bolton G, Jou LD, Dispensa BP et al.* Estimating the hemodynamic impact of interventional treatments of aneurysms: numerical simulation with experimental validation: technical case report. Neurosurgery 2006; 59: E429–430, author reply E429–E430

8 *Jou LD, Wong G, Dispensa B et al.* Correlation between lumenal geometry changes and hemodynamics in fusiform intracranial aneurysms. AJNR 2005; 26: 2357–2363

9 *Shojima M, Oshima M, Takagi K et al.* Magnitude and role of wall shear stress on cerebral aneurysm: computational fluid dynamic study of 20 middle cerebral artery aneurysms. Stroke, a journal of cerebral circulation 2004; 35: 2500–2505

10 *Castro MA, Putman CM, Cebral JR.* Patient-specific computational fluid dynamics modeling of anterior communicating artery aneurysms: a study of the sensitivity of intra-aneurysmal flow patterns to flow conditions in the carotid arteries. AJNR 2006; 27: 2061–2068

11 *Castro MA, Putman CM, Cebral JR.* Computational fluid dynamics modeling of intracranial aneurysms: effects of parent artery segmentation on intra-aneurysmal hemodynamics. AJNR 2006; 27: 1703–1709

12 *Castro MA, Putman CM, Cebral JR.* Patient-specific computational modeling of cerebral aneurysms with multiple avenues of flow from 3D rotational angiography images. Academic radiology 2006; 13: 811–821

13 *Cebral JR, Castro MA, Burgess JE et al.* Characterization of cerebral aneurysms for assessing risk of rupture by using patient-specific computational hemodynamics models. AJNR 2005; 26: 2550–2559

14 *Cebral JR, Lohner R.* Efficient simulation of blood flow past complex endovascular devices using an adaptive embedding technique. IEEE transactions on medical imaging 2005; 24: 468–476

15 *Cebral JR, Pergolizzi Jr RS, Putman CM.* Computational fluid dynamics modeling of intracranial aneurysms: qualitative comparison with cerebral angiography. Academic radiology 2007; 14: 804–813

16 *Karmonik C, Klucznik R, Benndorf G.* Blutfluss in zerebralen Aneurysmen: Vergleich von Phasen-Kontrast-Magnetresonanztomografie und Computational Fluid Dynamics – erste Erfahrungen. Fortschr Röntgenstr 2008; 180: 209–215

17 *Meyer FB, Huston 3rd J, Riederer SS.* Pulsatile increases in aneurysm size determined by cine phase-contrast MR angiography. Journal of neurosurgery 1993; 78: 879–883

18 *Ishida F, Ogawa H, Simizu T et al.* Visualizing the dynamics of cerebral aneurysms with four-dimensional computed tomographic angiography. Neurosurgery 2005; 57: 460–471, discussion 460–471

19 *Toth M, Nadasy GL, Nyary I et al.* Sterically inhomogenous viscoelastic behavior of human saccular cerebral aneurysms. Journal of Vascular Research 1998; 35: 345–355

20 *Steiger HJ, Aaslid R, Keller S et al.* Strength, elasticity and viscoelastic properties of cerebral aneurysms. Heart and vessels 1989; 5: 41–46

21 *Humphrey JD, Canham PB.* Structure, mechanical properties, and mechanics of intracranial saccular aneurysms. Journal of Elasticity 2000; 61: 49–81

22 *Challa V, Han HC.* Spatial variations in wall thickness, material stiffness and initial shape affect wall stress and shape of intracranial aneurysms. Neurological research 2007; 29: 569–577

23 *Hademenos GJ, Massoud T, Valentino DJ et al.* A nonlinear mathematical model for the development and rupture of intracranial saccular aneurysms. Neurological research 1994; 16: 376–384

24 *Baek S, Rajagopal KR, Humphrey JD.* A theoretical model of enlarging intracranial fusiform aneurysms. Journal of biomechanical engineering 2006; 128: 142–149

25 *David G, Humphrey JD.* Further evidence for the dynamic stability of intracranial saccular aneurysms. Journal of biomechanics 2003; 36: 1143–1150

26 *Haslach Jr HW.* A nonlinear dynamical mechanism for bruit generation by an intracranial saccular aneurysm. Journal of mathematical biology 2002; 45: 441–460

27 *Humphrey JD, Kyriacou SK.* The use of Laplace's equation in aneurysm mechanics. Neurological research 1996; 18: 204–208

28 *Kyriacou SK, Humphrey JD.* Influence of size, shape and properties on the mechanics of axisymmetric saccular aneurysms. Journal of biomechanics 1996; 29: 1015–1022

29 *Ryan JM, Humphrey JD.* Finite element based predictions of preferred material symmetries in saccular aneurysms. Ann Biomed Eng 1999; 27: 641–647

30 *Seshaiyer P, Humphrey JD.* On the potentially protective role of contact constraints on saccular aneurysms. Journal of biomechanics 2001; 34: 607–612

31 *Shah AD, Humphrey JD.* Finite strain elastodynamics of intracranial saccular aneurysms. Journal of biomechanics 1999; 32: 593–599

32 *Haacke EM, Li D, Kaushikkar S.* Cardiac MR imaging: principles and techniques. Top Magn Reson Imaging 1995; 7: 200–217

33 *Draney MT, Arko FR, Alley MT et al.* Quantification of vessel wall motion and cyclic strain using cine phase contrast MRI: in vivo validation in the porcine aorta. Magn Reson Med 2004; 52: 286–295

34 *Wedding KL, Draney MT, Herfkens RJ et al.* Measurement of vessel wall strain using cine phase contrast MRI. J Magn Reson Imaging 2002; 15: 418–428

35 *Yoshii S, Mohri N, Kamiya K et al.* Cine magnetic resonance imaging study of blood flow and wall motion of the aortic arch. Japanese circulation journal 1996; 60: 553–559

36 *Matsumoto Y, Honda T, Hamada M et al.* Evaluation of aortic distensibility in patients with coronary artery disease by use of cine magnetic resonance. Angiology 1996; 47: 149–155

37 *Zhao S, Croisille P, Janier M et al.* Comparison between qualitative and quantitative wall motion analyses using dipyridamole stress breath-hold cine magnetic resonance imaging in patients with severe coronary artery stenosis. Magnetic resonance imaging 1997; 15: 891–898

38 *Faries PL, Agarwal G, Lookstein R et al.* Use of cine magnetic resonance angiography in quantifying aneurysm pulsatility associated with endoleak. J Vasc Surg 2003; 38: 652–656

39 *Vos AW, Wisselink W, Marcus JT et al.* Aortic aneurysm pulsatile wall motion imaged by cine MRI: a tool to evaluate efficacy of endovascular aneurysm repair? Eur J Vasc Endovasc Surg 2002; 23: 158–161

40 *Vos AW, Wisselink W, Marcus JT et al.* Cine MRI assessment of aortic aneurysm dynamics before and after endovascular repair. J Endovasc Ther 2003; 10: 433–439

41 *Zhao M, Charbel FT, Alperin N et al.* Improved phase-contrast flow quantification by three-dimensional vessel localization. Magnetic resonance imaging 2000; 18: 697–706

42 *Abramoff MD.* Image Processing with ImageJ. Biophotonics International 2004; 11: 36–42

43 *Scott R, Atkins F, Harper PV.* Median Window Filter as a Smoothing-Edge Preserving Technique. Journal of Nuclear Medicine 1978; 19: 749–749

44 *Zhao M, Amin-Hanjani S, Ruland S et al.* Regional cerebral blood flow using quantitative MR angiography. AJNR 2007; 28: 1470–1473

45 *Monninghoff C, Maderwald S, Theysohn JM et al.* Beurteilung von intrakraniellen Hirnarterienaneurysmen mit 7 Tesla versus 1,5-Tesla-Time-

of-Flight-MR-Angiografie – erste Erfahrungen. Fortschr Röntgenstr 2009; 181: 16–23

46 *Hähnel S, Stippich C, Hartmann M et al.* Kraniale und zervikale arterielle Gefäßverletzungen: Bildgebung und Therapie. Fortschr Röntgenstr 2007; 179: 119–129

47 *Zhu W, Feng D, Qi J et al.* Evaluation of large intracranial aneurysms with cine MRA and 3D contrast-enhanced MRA. J Huazhong Univ Sci Technolog Med Sci 2004; 24: 95–98, 106

48 *MacDonald DJ, Finlay HM, Canham PB.* Directional wall strength in saccular brain aneurysms from polarized light microscopy. Ann Biomed Eng 2000; 28: 533–542

49 *San Millan Ruiz D, Yilmaz H, Dehdashti AR et al.* The perianeurysmal environment: influence on saccular aneurysm shape and rupture. AJNR 2006; 27: 504–512

50 *Dietrich U, Wanke I, Wittenberg G.* Rupturiertes Aneurysma bei Fenestration der distalen A. basilaris. Fortschr Röntgenstr 2008; 180: 255–257

51 *Moftakhar R, Aagaard-Kienitz B, Johnson K et al.* Noninvasive measurement of intra-aneurysmal pressure and flow pattern using phase contrast with vastly undersampled isotropic projection imaging. AJNR 2007; 28: 1710–1714

52 *Meckel S, Stalder AF, Santini F et al.* In vivo visualization and analysis of 3-D hemodynamics in cerebral aneurysms with flow-sensitized 4-D MR imaging at 3T. Neuroradiology 2008; 50(6): 473–484

53 *Frydrychowicz A, Markl M, Harloff A et al.* Die Analyse aortaler Hamodynamik und Gefasswandparameter mittels fluss-sensitiver in-vivo 4D-MRT bei 3 Tesla. Fortschr Röntgenstr 2007; 179: 463–472